mathematics

Article

Seismic Response and Damage Characteristics of RCC Gravity Dams Considering Weak Layers Based on the Cohesive Model

Gaohui Wang [1,2], Aobo Liu [1,2,*], Wenbo Lu [1,2], Ming Chen [1,2] and Peng Yan [1,2]

[1] State Key Laboratory of Water Resources and Hydropower Engineering Science, Wuhan University, Wuhan 430072, China
[2] Key Laboratory of Rock Mechanics in Hydraulic Structural Engineering, Ministry of Education, Wuhan University, Wuhan 430072, China
* Correspondence: liuaobo@whu.edu.cn

Abstract: Due to the construction technology of roller compacted concrete (RCC) gravity dams, there are many weak layers that have the potential to affect the seismic performance of dams. However, research on the seismic response and failure characteristics of RCC dams considering their layered characteristic is still lacking. In this paper, the zero-thickness cohesive element is presented to model the mechanical behavior of the RCC layers. An impacted concrete beam is selected to verify its effects on simulating crack propagation. Subsequently, the concrete damaged plasticity model is utilized to model concrete under seismic loading. The dynamic interaction in the gravity dam-reservoir-foundation system is considered by coupled acoustic-structural method, whose rationality is validated by seismic failure mode analysis of the Koyna dam under the 1967 Koyna earthquake. The validated algorithms are applied to investigate the influence of the weak layer at different elevations on the seismic response and the failure process of the Guandi RCC gravity dam. On this basis, the effects of well-bonded RCC layers set at intervals along the dam on the nonlinear response and failure modes under strong earthquakes are further investigated. The results reveal that the weak layer will influence the anti-seismic capacity of RCC gravity dams, and the damage characteristics of the dam are significantly changed. In addition, well-bonded RCC layers still affect the seismic response of RCC gravity dams. Increasing displacement response and energy dissipation can be observed. Meanwhile, RCC layers lead to more severe damage to the dam under the same seismic input.

Keywords: RCC gravity dam; weak layer; cohesive model; coupled acoustic-structural method; seismic performance

MSC: 37M10

Citation: Wang, G.; Liu, A.; Lu, W.; Chen, M.; Yan, P. Seismic Response and Damage Characteristics of RCC Gravity Dams Considering Weak Layers Based on the Cohesive Model. *Mathematics* **2023**, *11*, 1567. https://doi.org/10.3390/math11071567

Academic Editor: Elena Benvenuti

Received: 27 February 2023
Revised: 21 March 2023
Accepted: 22 March 2023
Published: 23 March 2023

1. Introduction

Because of their advantages regarding relatively simpler and faster construction, lower costs, and better environmental adaptability, roller compacted concrete (RCC) dams have been widely used around the world. Different from normal concrete dams, RCC dams are usually built in thin and horizontal lifts [1]. In general, the thickness of each RCC layer is 30cm [2], and concreting lifts are usually placed every 3.0 m to satisfy the construction requirements [3]. As a result of its special construction technology, weak interfaces may occur during construction. There may be defects in the interlayers due to the lower cementation quality [3], which will have a nonnegligible impact on the dam's dynamic response and failure mechanism. Therefore, carrying out research on the seismic characteristics of RCC gravity dams considering construction layers under earthquakes is of great theoretical significance and engineering value.

Many researchers have conducted seismic response and failure behavior analysis with regard to normal concrete dams using different methods. The discrete crack model (DCM) and smeared crack model (SCM) are two traditional finite element models (FEMs). Ayari et al. [4] proposed a model to analyze the crack evolution of the Koyna dam based on DCM and fracture mechanics. Bhattacharjee and Leger [5] performed seismic analyses of the Koyna dam using a coaxial rotating crack model (CRCM). In addition, the damage theory is also a robust tool. The concrete damaged plasticity (CDP) model was employed by Lee and Fevens [6] to analyze the Koyna dam's failure mode. Daneshyar and Ghaemian [7] improved the model to create a rate-dependent anisotropic model. Tidke and Adhikary [8] used the CDP model to conduct incremental dynamic analysis (IDA) of the Koyna dam considering the effects of layered foundation. Recently, the extended finite element method (XFEM) has been applied to seismic analysis to address the issues with remeshing in the FEM. Wang et al. [9] used the XFEM to examine the Guandi concrete gravity dam's possible failure modes. Wang et al. [10] carried out crack analyses on a concrete gravity dam under seismic load with different initial crack cases by employing the XFEM. Haghani et al. [11,12] developed a model coupling the XFEM with time integration using the α-method and applied it to gravity dams to obtain the dynamic fracture results. Haghani et al. [13] also compared the differences between SCM and XFEM in simulating the dam's crack process. In addition, there are other models for the failure simulation of dams. Mirzayee, Khaji, and Ahmadi [14] modeled and studied the seismic response of the cracked concrete gravity dam using the hybrid distinct element-boundary element (DE-BE). Sharma, Fujisawa, and Murakami [15] utilized a space-time FEM to simulate the seismic responses of the Koyna dam. Wang et al. [16] proposed a generic numerical algorithm to estimate the crack growth process of concrete gravity dams under seismic loads.

It is noteworthy that most studies on the seismic response of the dams are more focused on normal concrete dams, while the layered characteristics of RCC dams are usually simply neglected, or RCC dams are regarded in an approached way, similarly to normal concrete dams [1,9,10,16–21], with few exceptions. As for RCC dams, there may be weak bonding surfaces among compacted layers due to material properties, construction technology, climate conditions, and other uncertain factors. Therefore, cracks are likely to occur along the interface, which may affect the seismic responses of the dam. Many contributions have investigated the effect of certain construction layers on the structural behavior of the RCC dam. For instance, Zhao and Li [1] considered both the interface between the dam and the foundation and the interface between the two RCC materials of the dam in a seismic analysis of the dam. Sha, Lei, and Zhang [22] discussed the Huangdeng RCC gravity dam's failure mechanism using an isotropic damage model. However, the impact of RCC layers on the seismic responses of dams has not been examined. Therefore, the present work aims to study the influence of layered characteristics on the seismic response and damage characteristics of RCC dams.

The key to investigating the seismic performance of RCC dams is selecting an effective and efficient model to simulate the weak layers. Among various models simulating interfaces, the zero-thickness cohesive element model is useful in describing the failure behavior of boned interfaces. The cohesive model (CM) was originally used in fracture mechanics analysis of materials such as polymers, metals, and composites [23,24]. Later, the CM was further extended to simulate the bonded interfaces and approximate nonlinear fracture problems of concrete by Hillerborg, Modéer, and Petersson [25]. Since then, the CM has been commonly applied to quasi-brittle materials such as concrete [26,27] and implemented for concrete dams. For instance, Paggi, Ferro, and Braga [28] and Zhong et al. [29] both studied the response of the interface between the dam and the foundation. The results all indicated the effectiveness and accuracy of the CM. Zhu et al. [30] also used the CM to simulate the discontinuous foundation and the dam-foundation interface. The results were contrasted with those of the elastic and plastic models to further demonstrate the cohesive model's validity. Generally, the CM has been widely used in simulating different kinds of interfaces. However, the CM has not been used to study the layered characteristic of the RCC dam.

Another concern in the seismic analysis of dams is the dynamic interactions in the dam-foundation-reservoir system [31,32]. The coupled acoustic-structural method [8,19,33] provides an alternative approach for seismic response analysis of large-scale models, which can effectively and accurately solve the problem of fluid-structure interaction. Hence, the coupled acoustic-structural method has been widely used in the dynamic response analysis of structures under earthquakes.

Considering the vital importance of the anti-seismic capacity of RCC gravity dams, and the deficiency of neglecting the effects of construction layers in the existing literature, the present study aims to investigate the influence of the RCC layer on the seismic responses of RCC dams. The zero-thickness cohesive element model was used to simulate the construction layers, which was verified by an experiment on an impacted concrete beam with an initial crack, discussed in Section 2. Additionally, the gravity dam-reservoir-foundation system's dynamic interaction is described using the coupled acoustic-structural method, as introduced in Section 3. By comparing the Koyna dam's failure modes obtained by this method with the existing experimental scaled-down results, its validity is proven. Section 4 gives detailed descriptions of the simulation, including the finite element model and calculation parameters of the Guandi RCC gravity dam. Then the seismic responses and failure characteristics of the Guandi dam with a weak layer located in different elevations are carried out in Section 5 to identify its effects. Ultimately, the influence of well-bonded RCC layers set with a certain interval along the dam on the RCC gravity dam is discussed in Section 6.

2. Cohesive Model

The cohesive model is a robust method used to model bonded interfaces and approximate the failure behavior as the result of the loading. It is applied in ABAQUS and can be realized depending on element-based cohesive elements or surface-based cohesive behavior, which equals zero-thickness cohesive elements. The constitutive relation of the model contains the traction-separation law described by initial stiffness, damage initiation criterion, and damage evolution law [26]. The constitutive relations between traction and separation can be divided into four types, which are bilinear, trapezoidal, parabolic, and exponential. Figure 1 illustrates the bilinear constitutive relation, which is the most commonly used type with high computational efficiency [34]. The specific descriptions and definitions of this constitutive relationship are detailed in the following paragraphs.

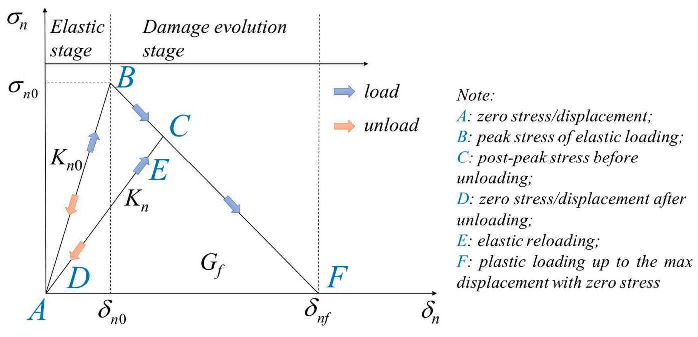

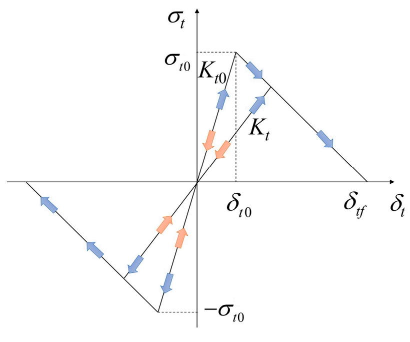

Figure 1. Bilinear constitutive relation between traction and separation. (**a**) Normal direction; (**b**) shear direction.

2.1. Initial Stiffness

It is clear from Figure 1 that the initial response is assumed to be elastic. The traction increases when the relative displacement increases with an initial stiffness. The definition of stress in the elasticity stage is:

$$\boldsymbol{\sigma} = \begin{Bmatrix} \sigma_n \\ \sigma_s \\ \sigma_t \end{Bmatrix} = \boldsymbol{K} \begin{Bmatrix} \delta_n \\ \delta_s \\ \delta_t \end{Bmatrix} = \boldsymbol{K}\delta \quad (1)$$

$$\boldsymbol{K} = \mathrm{diag}(K_{n0} \quad K_{t0} \quad K_{s0}) \tag{2}$$

where $\boldsymbol{\sigma}$ is the interfacial strength, and σ_n, σ_s, and σ_t are the nominal stresses when the deformation is either purely normal to the interface or purely in the first or the second shear direction, respectively. Failure in the pure n-direction corresponds to Mode I tensile failure in fracture mechanics; failure in the directions of s and t correspond to Mode II and III failure under shear stress in fracture mechanics. [35]. δ_n, δ_s, and δ_t are the corresponding displacements, and K_{n0}, K_{t0}, and K_{s0} are the initial normal and two shear elastic moduli, respectively.

It is noted that the units of K and δ are Pa/m and m in the SI system, respectively. For zero-thickness cohesive elements in ABAQUS [36], the default constitutive thickness is 1, which ensures that the nominal strain is equal to the separation and the stiffness is equal to the elastic modulus numerically.

2.2. Damage Initiation Criterion

The damage initiation criterion refers to the moment at which the cohesive response starts to degrade. The damage initiation point δ_0 corresponds to the peak value of the traction-separation curve. At the time when $\delta > \delta_0$, the damage begins, and the stiffness of the material degrades from K_0 to K.

There are different damage initiation criteria defined by stress or displacement, i.e., the maximum stress criterion, the maximum separation criterion, the quadratic stress criterion, and the quadratic separation criterion. The criterion should be selected according to key factors such as material characteristics, research objectives, and so on. The maximum nominal stress criterion is used in this paper, which means that damage begins to occur when the maximum contact stress ratio reaches a value of 1. The following is a representation of this criterion:

$$\max\left\{\frac{\langle\sigma_n\rangle}{\sigma_{n0}}, \frac{\sigma_s}{\sigma_{s0}}, \frac{\sigma_t}{\sigma_{t0}}\right\} = 1 \tag{3}$$

where σ_{n0}, σ_{s0}, and σ_{t0} illustrate the peak contact stress when the separation is only normal to the interface, solely in the first shear direction, or purely in the second shear direction, respectively. The McCauley brackets signify that only positive values are considered, irrespective of a purely compressive stress state.

$$\langle\sigma_n\rangle = \begin{cases} \sigma_n, & \sigma_n \geq 0 \\ 0, & \sigma_n < 0 \end{cases} \tag{4}$$

The quadratic stress criterion is also often used to determine the damage initiation. When the contact stress ratio reaches a value of 1, damage begins. This criterion can be expressed by the following representation:

$$\left\{\frac{\langle\sigma_n\rangle}{\sigma_{n0}}\right\}^2 + \left\{\frac{\sigma_s}{\sigma_{s0}}\right\}^2 + \left\{\frac{\sigma_t}{\sigma_{t0}}\right\}^2 = 1 \tag{5}$$

2.3. Damage Evolution Law

The damage evolution law is used to describe the stiffness degradation when damage begins, and the damage factor d is often used to express the degree of degradation.

$$\boldsymbol{\sigma} = \begin{Bmatrix} \sigma_n \\ \sigma_s \\ \sigma_t \end{Bmatrix} = (1-d)\boldsymbol{K}\begin{Bmatrix} \delta_n \\ \delta_s \\ \delta_t \end{Bmatrix} + d\boldsymbol{K}\begin{Bmatrix} \langle -\delta_n\rangle \\ 0 \\ 0 \end{Bmatrix} \tag{6}$$

where the damage factor d indicates the degree of damage. The value of d varies monotonically between 0 and 1 when the damage starts. $d = 0$ represents that the material is not damaged, and $d = 1$ means complete damage to the material.

One way to define factor d is the effective displacement δ_m [37]. The linear damage evolution law is shown below:

$$d = \frac{\delta_{mf}(\delta_{m\max} - \delta_{m0})}{\delta_{m\max}(\delta_{mf} - \delta_{m0})} \tag{7}$$

$$\delta_m = \sqrt{\langle \delta_n \rangle^2 + \delta_s^2 + \delta_t^2} \tag{8}$$

where δ_{m0} is the initial cracking displacement, $\delta_{m\max}$ is the maximum effective displacement, and δ_{mf} is the displacement when the cohesive response has completely failed. The details of this definition of the damage factor are available in [35,37].

Another way to describe damage evolution is fracture energy. The energy required to form a unit area of the fracture surface is referred to as fracture energy. Figure 1 shows that the fracture energy is equivalent to the area within the traction-separation curve.

$$G = \int_0^{\delta_f} \sigma(\delta)\mathrm{d}\delta = \frac{1}{2}\sigma_{n0}\delta_f \tag{9}$$

where σ_{n0} is the cohesion strength. Energy-based damage evolution is more widely used because the fracture energy of dam concrete is easier to obtain and there have been many empirical formulas for approximately calculating fracture energy. As a result, energy-based damage evolution is utilized in the present study.

2.4. Validation Test

A typical impact test of a concrete beam with an initial crack conducted by Du et al. [38] is used herein to verify the cohesive model. The basic data from the experiment are shown in Figure 2. In the finite element model, the element type of the cohesive elements was COH3D8 (8-node three-dimensional cohesive element.), and that of other parts was C3D8R (8-node three-dimensional solid element). Both ends of the beam were fixed, and the load was applied in the middle of the top face.

Figure 2. Impact test of a concrete beam. (**a**) Geometry (Unit: mm); (**b**) FE model.

The concrete properties were as follows: the elasticity modulus E = 34.48 GPa, the mass density ρ = 2500 kg/m^3, the Poisson's ratio ν = 0.2, the tensile strength f = 5.24 MPa, and the fracture energy G = 200 N/m. The cohesive elements were set along the area where it was possible for the fracture to occur in consideration of the symmetry of the system. The bilinear traction-separation law was used. It was assumed that if the stress of the concrete in a certain direction exceeds the strength, the damage would begin and the stiffness starts to degrade. Hence, the maximum principal stress damage initiation criterion was adopted. Considering the available parameters, the energy-based damage evolution with linear softening was selected. The impact load history obtained from the test is shown in Figure 3.

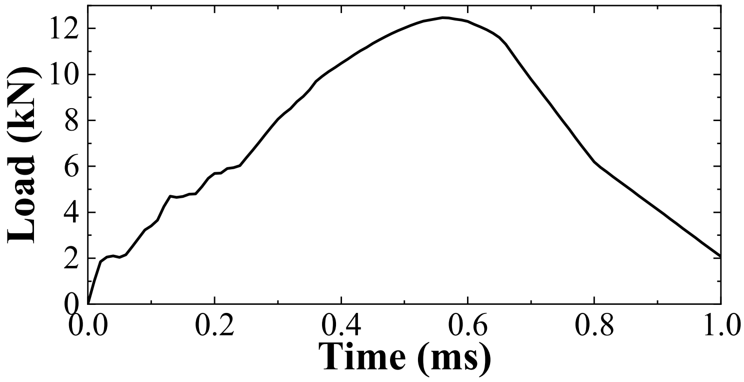

Figure 3. Load history used for the impact test.

Figure 4a displays the computational and experimental results of the crack extension. Figure 4b compares the experimental results to the calculated relationship between the load and the vertical displacement at the loading point. The results obtained from simulations based on the fracture process zone (FPZ) model [38], Drucker-Prager elastoplastic (DP) model [39], and explicit scaled boundary FEM(SBFEM)-FEM [40] are also plotted. Obviously, the results of the numerical and experimental simulations agree well. It is noted that there are some errors, probably caused by complex issues such as discretization, model assumptions of concrete properties, and so on. This example demonstrates that the cohesive model has a good simulation effect on crack propagation.

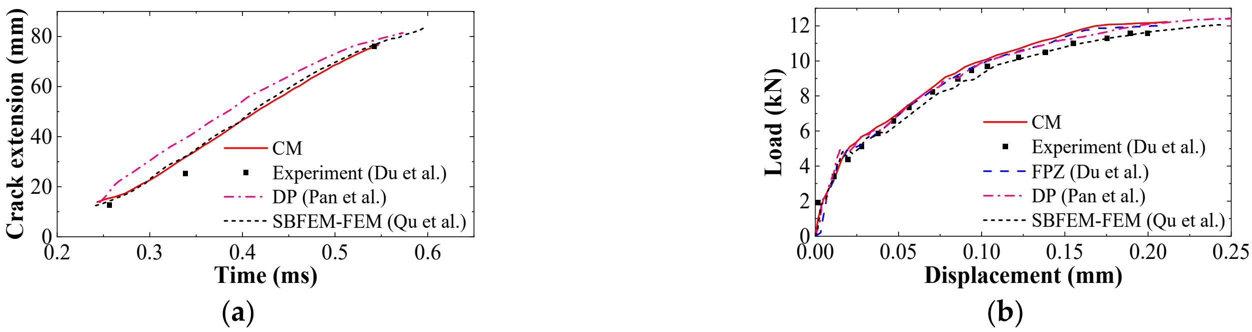

Figure 4. Comparison between numerical simulation and existing research results [38–40]. (**a**) Crack extension history; (**b**) load-vertical displacement curves at the loading point.

3. The Coupled Acoustic-Structural Method

The coupled acoustic-structural method, which can solve the problems of dynamic interactions, has been applied in ABAQUS. In the coupled acoustic-structural method, fluid (air, water, etc.) is approximated by the linear acoustic element, in which there is only pressure related to the volumetric strain and no shear stress. Hence, the method can be used to model a coupled fluid-structural system with high calculation precision. The method used in the gravity dam-reservoir-foundation system is shown schematically in Figure 5.

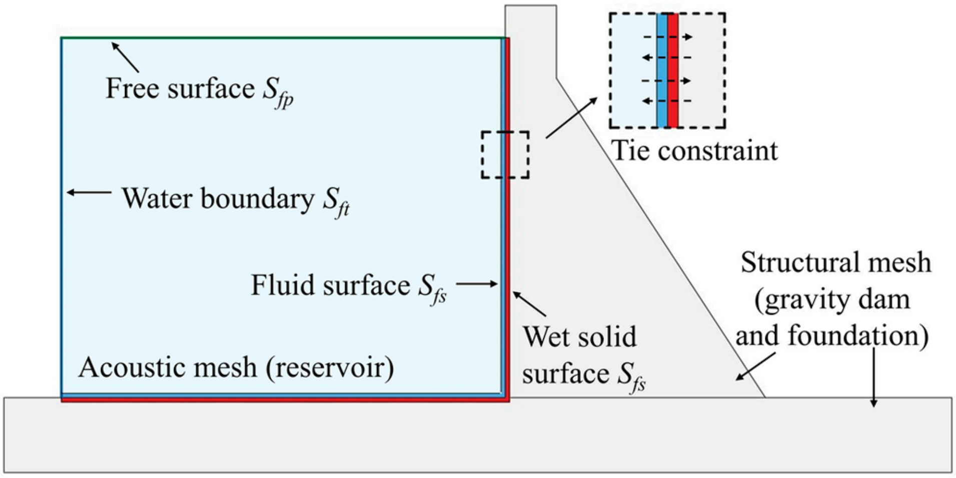

Figure 5. The coupled acoustic-structural method.

3.1. Assumptions about the Acoustic Medium

For the tiny motion of the compressible and inviscid fluid, the method uses an equilibrium equation to describe the acoustic medium. The equation is shown below.

$$\frac{\partial p}{\partial \mathbf{x}} + \gamma \dot{\mathbf{u}}^f + \rho_f \ddot{\mathbf{u}}^f = 0 \tag{10}$$

where p is the dynamic pressure of the fluid, x is the fluid particle's position in space, $\dot{\mathbf{u}}^f$ is its velocity, $\ddot{\mathbf{u}}^f$ is its acceleration, ρ_f is the fluid's density, and γ is the volume resistance generated when the fluid flows through the matrix material.

By assuming that the constitutive behavior of the fluid is inviscid and compressible, the bulk modulus of the acoustic medium is related to the dynamic pressure and volume strain in the medium.

$$p = -K_f \varepsilon_V \tag{11}$$

where $\varepsilon_V = \varepsilon_{11} + \varepsilon_{22} + \varepsilon_{33}$ is volumetric strain, and K_f is the bulk modulus.

3.2. Formulation for Direct Integration Transient Dynamics

The characteristics of acoustic fields are closely related to the boundary conditions. The boundary of the acoustic medium region conforming to Equations (10) and (11) is divided into subregions S. Based on these two equations, the motion equation with the form of sound pressure p can be obtained as below:

$$\frac{1}{K_f}\ddot{p} + \frac{\gamma}{\rho_f K_f}\dot{p} - \frac{\partial}{\partial \mathbf{x}}\left(\frac{1}{\rho_f}\frac{\partial p}{\partial \mathbf{x}}\right) = 0 \tag{12}$$

It is assumed that p is on S_{fp}, and Equation (10) is used on the remainder of the boundary S-S_{fp}. The relationship between pressure gradient and boundary motion of fluid can be obtained from Equation (10):

$$\mathbf{n}^-\left(\frac{1}{\rho_f}\frac{\partial p}{\partial \mathbf{x}} + \frac{\gamma}{\rho_f}\dot{\mathbf{u}}^f + \ddot{\mathbf{u}}^f\right) = 0 \tag{13}$$

where $\mathbf{n}^-$ represents the internal normal direction of the fluid boundary. In order to describe various boundary conditions more simply, the boundary traction term $T(\mathbf{x}) = -\mathbf{n}^- \cdot \left(\frac{1}{\rho_f}\frac{\partial p}{\partial \mathbf{x}}\right)$ is introduced.

All boundary conditions can be expressed by $T(\mathbf{x})$, except for the boundary condition S_{fp} for directly specifying acoustic pressure. S_{fp} is often used to set the boundary condition of the reservoir surface. When the acoustic pressure on the surface of the reservoir is set to 0, the effect of the surface wave of the water is ignored.

The radiating boundary S_{ft} is often used for the truncated far end of the reservoir domain. It can be applied by specifying the corresponding impedance:

$$T_{ft}(\mathbf{x}) = -\left(\frac{1}{c_1}\dot{p} + \frac{1}{a_1}p\right) \tag{14}$$

where $\frac{1}{c_1} = \left[\frac{f}{\sqrt{\rho_f K_f}}\right]$ and $\frac{1}{a_1} = f\left[\frac{\beta}{\rho_f} + \frac{\gamma}{2\rho_f\sqrt{\rho_f K_f}}\right]$.

The acoustic-structural interface S_{fs} refers to the coupling boundary between fluid and structure, on which the normal displacement of two materials is equal, i.e.,

$$\mathbf{n}^- \cdot \mathbf{u}^f = \mathbf{n}^- \cdot \mathbf{u}^m \tag{15}$$

where $\mathbf{u}^f$ and $\mathbf{u}^m$ are the displacement of fluid and structure, respectively. Following from this, the acoustic boundary traction coupling fluid to solid is depicted below when volumetric drag is present.

$$T_{fs}(x) = \mathbf{n}^-\left(\ddot{\mathbf{u}}^m + \frac{\gamma}{\rho_f}\dot{\mathbf{u}}^m\right) \tag{16}$$

3.3. Verification Test

In order to confirm the reliability of the method, the damage behavior of the Koyna concrete gravity dam was studied under the 1967 Koyna earthquake. The acceleration time history of the Koyna seismic wave is shown in Figure 6. Only horizontal and vertical components of the seismic ground motions were considered in the validation test. The finite element mesh of the two-dimensional model established in the software ABAQUS is shown in Figure 7. An upstream reservoir level of 96.5 m was considered. Since the focus of this part was to verify the rationality of the coupling method of reservoir and dam, the foundation extended the distance of the dam height in the downstream and depth direction, and two times the dam height in the upstream direction.

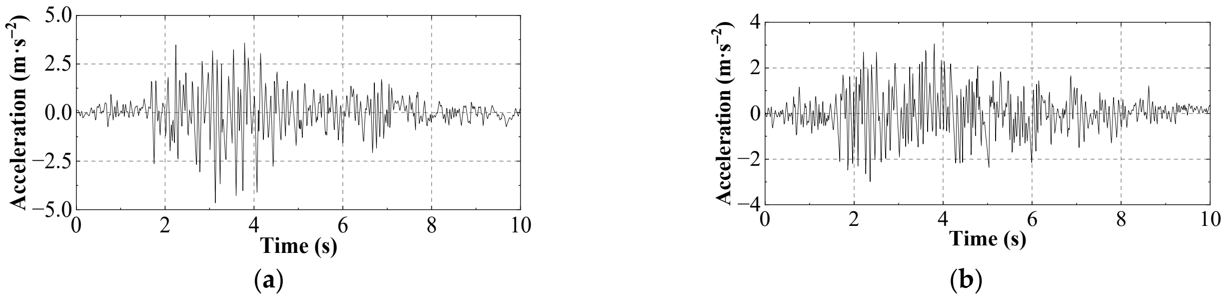

Figure 6. Koyna earthquake accelerations. (**a**) Horizontal component; (**b**) vertical component.

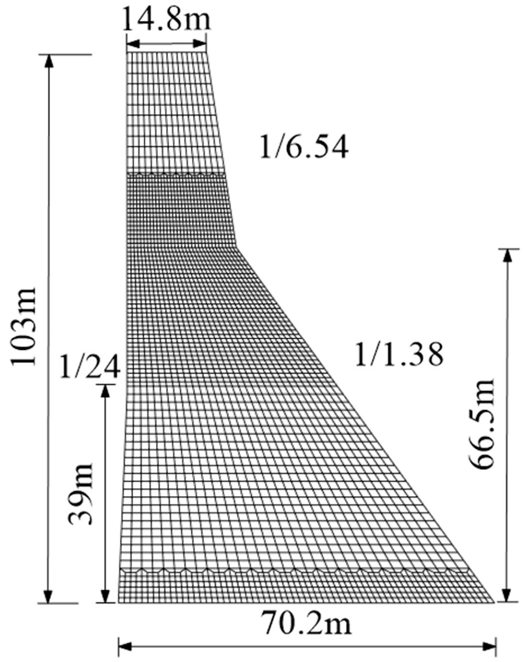

Figure 7. Detailed plot of the 2D FE model of the Koyna dam.

The concrete parameters of the dam were as follows [41]: the elasticity modulus E = 31.0 GPa, the mass density ρ = 2643 kg/m^3, and the Poisson's ratio ν = 0.2. The CDP model was used to describe the nonlinear characteristics of concrete. The CDP model was first developed by Lublinear et al. [42] and modified by Lee and Fevens [6]. The details of the CDP model can be found in the literature [43–45]. The tensile strength of concrete was 2.9 MPa and the compressive strength was 24.1 MPa. To minimize wave propagation effects, the foundation was assumed to be massless. The elasticity modulus of the foundation rock was 22.5 GPa. The dynamic interaction of the system was modeled by the coupled acoustic-structural method. The density of the water was 1000 kg/m^3 and the bulk modulus was 2.04 GPa. The Rayleigh damping method with a 5% damping ratio was used to calculate the energy dissipation of the system.

For the initial time step, it was assumed that the normal displacement of the truncated boundary was zero. Additionally, the boundaries of the foundation were completely constrained. Subsequently, all displacement restraints were relieved. Then the Koyna earthquake accelerations were applied to the foundation. The incremental dynamic analysis of time steps was calculated using the implicit Newmark-β integration method. The initial and maximum incremental steps were set to 0.01 s for high integration accuracy and efficiency. During the calculation, the reservoir water surface was regarded as a static surface, and tie constraints were used for the dam-reservoir coupling surface and the bottom of the reservoir.

Figure 8 shows the final damage profiles of the Koyna dam obtained from the 2D numerical simulation, existing research results and the model test. It can be seen that the failure mode of the dam obtained by the coupled acoustic-structural method is basically consistent with the result from the model test [46] and coupled Lagrange-Euler method [43]. A crack penetrating the whole section of the dam formed. Hydrodynamic pressure also caused cracks in the dam's intermediate zone on the upstream side. Therefore, the coupled acoustic-structural method can effectively simulate the dynamic interaction between the dam and reservoir.

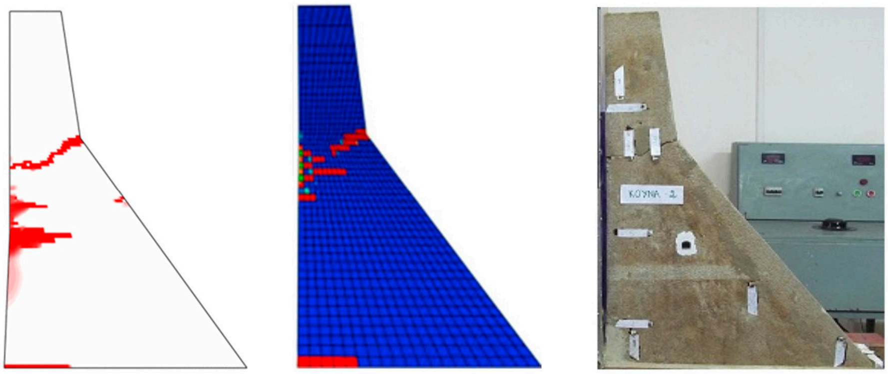

(**a**) (**b**) (**c**)

Figure 8. Final failure modes based on: (**a**) coupled acoustic-structural method; (**b**) coupled Lagrange-Euler method [43]; (**c**) experimental results from the model test [46].

4. Guandi RCC Gravity Dam-Reservoir-Foundation System

4.1. Guandi RCC Gravity Dam and Finite Element Model

The Guandi Hydropower Station is located in the lower reaches of the Yalong River, Sichuan Province, China. The water-retaining structure of the Guandi hydropower station is a typical RCC gravity dam, with a highest monolith of 168 m, a maximum thickness of the dam base of 153.2 m, and a crest length of 516.0 m. The representative value of the horizontal seismic peak ground acceleration (PGA) of the dam site is 0.34g (g = 9.81 m/s^2) [9], as per the Chinese seismic codes now in effect.

A typical non-overflow monolith with a height of 142 m and a dam base of 121 m was modeled. The FE mesh model of the Guandi RCC dam-reservoir-foundation system was established in ABAQUS, as shown in Figure 9a. The coordinate origin is the lower left corner of the dam. The level of reservoir water is 138 m. In both the upstream and downstream directions, the foundation stretches for 1.5 times the height of the dam, and twice the height of the dam in the downward direction. The coupled acoustic-structural method was utilized, as in the previous section. On the basis of mesh sensitivity analysis [20,47], mesh sizes along the base and near the slope change were 1.0 m and 0.5 m, respectively, in which crack propagations were expected. The element size for other parts was about 1.5 m. The total number of elements in the dam was 6720.

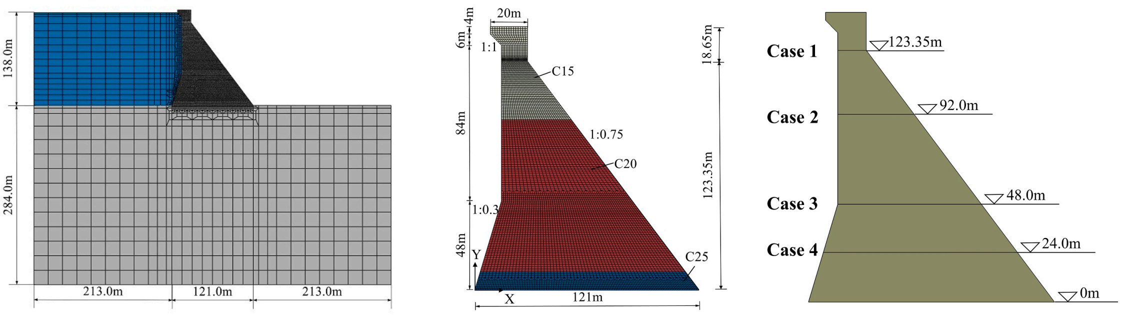

(**a**) (**b**) (**c**)

Figure 9. FE model of Guandi RCC dam-reservoir-foundation system. (**a**) 2D model of the system; (**b**) detailed plot of the dam; (**c**) four cases with different locations of RCC layers.

The zero-thickness cohesive element method was used in this section to simulate the properties of weak RCC interlayers. It was assumed that the weak layer would appear occasionally during construction. The weak layer was set at four different elevations to investigate its effects on the seismic responses of the dam. Four cases were considered, as shown in Figure 9c. The weak layers at 48.0 m elevation and 123.35 m elevation were at the level where the upstream and downstream slopes change abruptly. The layer at 92.0 m elevation was the interface between two materials, C15 and C20, which was one of the weakest surfaces among the most unfavorable layers [1]. Additionally, the layer at 24.0 m elevation was in the center of the dam's lower section.

4.2. Material Parameters

The properties of the three kinds of concrete in the dam are listed in Table 1 [9]. It is noted that the dynamic strength and modulus of concrete are 30% greater than the static parameters under the requirements of China's Code for Seismic Design of Hydraulic Structures [48], and the dynamic tensile strength is 10% of the dynamic compressive strength. The CDP model is used to describe the nonlinearity of concrete. The elastic modulus of the foundation rock is considered to be 21.6 GPa, with a Poisson's ratio of 0.2, and it is also assumed to be massless and linearly elastic. It is believed that a massless foundation prevents vibrations from the foundation base to the ground from being amplified. The parameters of the reservoir are the same as those in the verification test. According to the requirements of China's Code for Seismic Design of Hydraulic Structures [48] and relevant research practices [3,8–10,15,16,18,19,31,39,41], the energy dissipation of the system is characterized by the Rayleigh damping matrix deliberating the damping ratio of 5%.

Table 1. Concrete properties of the Guandi gravity dam.

Concrete	Density (kg/m^3)	Modulus (GPa)	Tensile Strength (Mpa)	Compressive Strength (Mpa)	Poisson's Ratio	Fracture Energy (N/m)
C15	2552	56.0	1.45	14.53	0.167	205
C20	2552	57.6	1.94	19.38	0.167	257
C25	2552	58.8	2.42	24.23	0.167	300

As for the zero-thickness cohesive elements, the contact property is defined as hard contact in the normal direction, and the friction coefficient in the tangential direction is 1.1, based on the standard values of concrete shear strength parameters in the Chinese design code for concrete gravity dams. Because of the lack of experimental data, the stiffness and the peak value of contact stress are chosen to be about 75% of the elastic modulus and tensile strength of the RCC noumenon, respectively [3]. The fracture energy of the weak interlayer is also taken as 75% of the fracture energy of the RCC body. The damage initiation of the interlayers is determined by the maximum principal stress criterion.

4.3. Loadings and Methods

In the initial step of static analysis, the self-weight of the dam and hydrostatic force was applied. The boundary conditions were the same as those in Section 3.3. It is worth noting that sediment pressure, uplift pressure, and temperature stress are not considered herein. Many researchers [19,26,49] have taken the same approach since these parameters have relatively little influence on the way the dam responds. All displacement constraints were removed for the subsequent step of dynamic analysis, and the seismic input was applied. The hydrodynamic pressure was considered based on the coupled acoustic-structural method. During the process, the surface of the reservoir was regarded as static, and tie constraints were used for the dam-reservoir coupling surface and the reservoir bottom. The seismic response analysis was carried out using the implicit Newmark-β time integration approach. The initial and maximum increment steps were 0.01 s. The 1967 Koyna #Koyna dam earthquake was utilized as the ground motion input as there are no actual earthquake recordings from the region around the dam. According to the requirements from China's Code for Seismic Design of Hydraulic Structures [48], the original horizontal acceleration components were rescaled to match the design peak acceleration while the vertical PGA is 2/3 of the horizontal value. Additionally, the seismic waves were processed to reduce the errors between their spectral characteristics and those of the standard design response spectrum.

5. Nonlinear Dynamic Response and Damage Characteristics of Guandi RCC Gravity Dam Considering a Weak Layer

5.1. Analysis of Nonlinear Dynamic Response Characteristics

Dynamic response analyses of the Guandi RCC gravity dam in different cases have been conducted. For assessing the effects of the weak layer on the dam dynamic response, the displacement of the dam crest is used for illustration. The relative displacement of the dam crest corresponding to the dam heel in four cases is shown in Figures 10 and 11 as follows, where the positive values represent that the dam deformed downstream and rose; otherwise it moved in the upstream direction and sunk. The sliding histories of the block of the dam above the weak layer are shown in Figure 12. From the results obtained, it can be concluded that the displacement responses of the dam crest are affected by the weak layer. Compared to the normal concrete dam, a larger peak displacement and residual deformation can be observed for the dam with a weak layer. In Case 1, the displacement responses in horizontal and vertical directions increase significantly because the dam neck is one of the weakest links of the dam. In Case 2, the weak layer is located at the interface between two concrete materials. As can be seen in Figure 12, the movement of the upper dam block is mainly manifested by sliding along the weak layer, so the variation amplitude of horizontal displacement is much larger than that of vertical displacement. Meanwhile, the dam block at the upper part of the weak layer swings back and forth under the earthquake in Case 3 and Case 4 because the rigidity of the lower part of the dam body is relatively higher. As a result, the horizontal displacement of the dam crest and the sliding displacement along the layer in these two cases are smaller than those in the former two cases. Meanwhile, the vertical displacement of the dam crest has more obvious changes, and the residual deformation implies that the dam head sinks after the earthquake in Case 3 and Case 4.

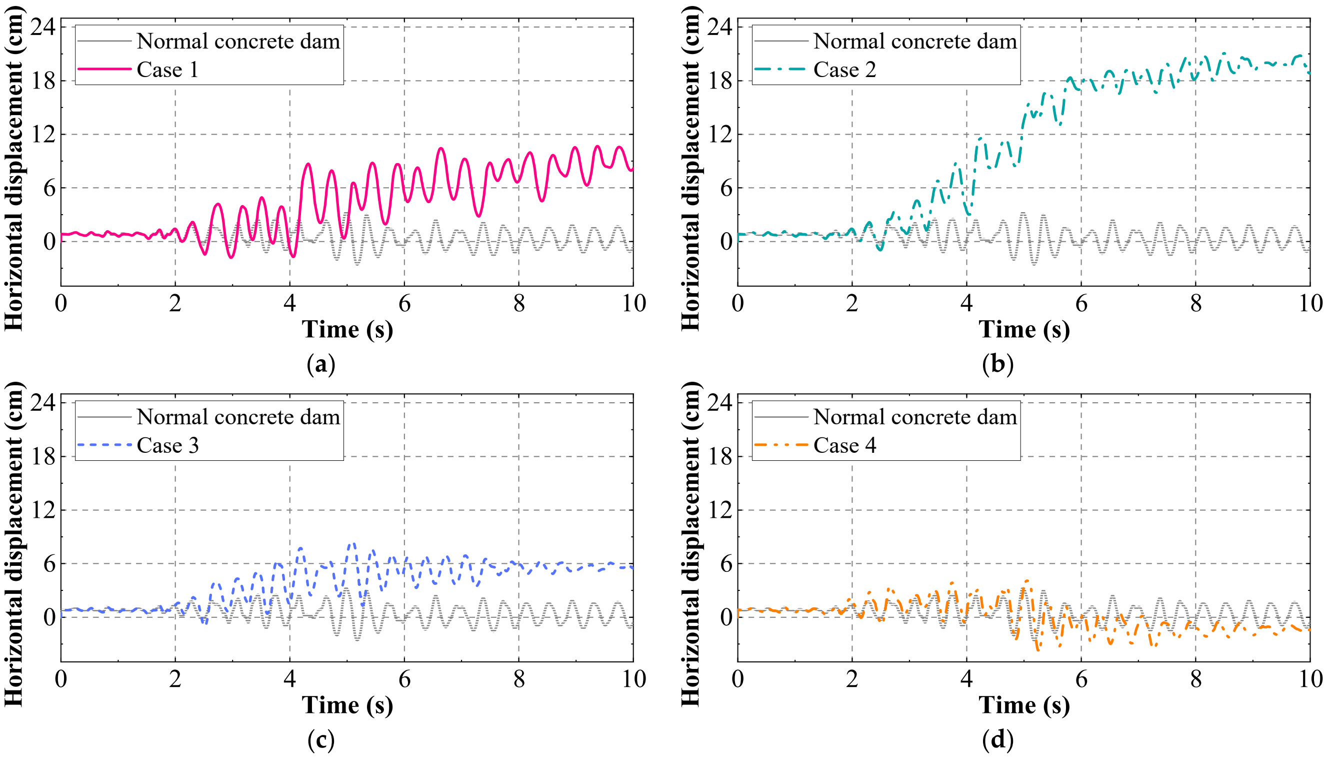

Figure 10. Horizontal displacement responses of the dam crest. (**a**) Case 1; (**b**) Case 2; (**c**) Case 3; (**d**) Case 4.

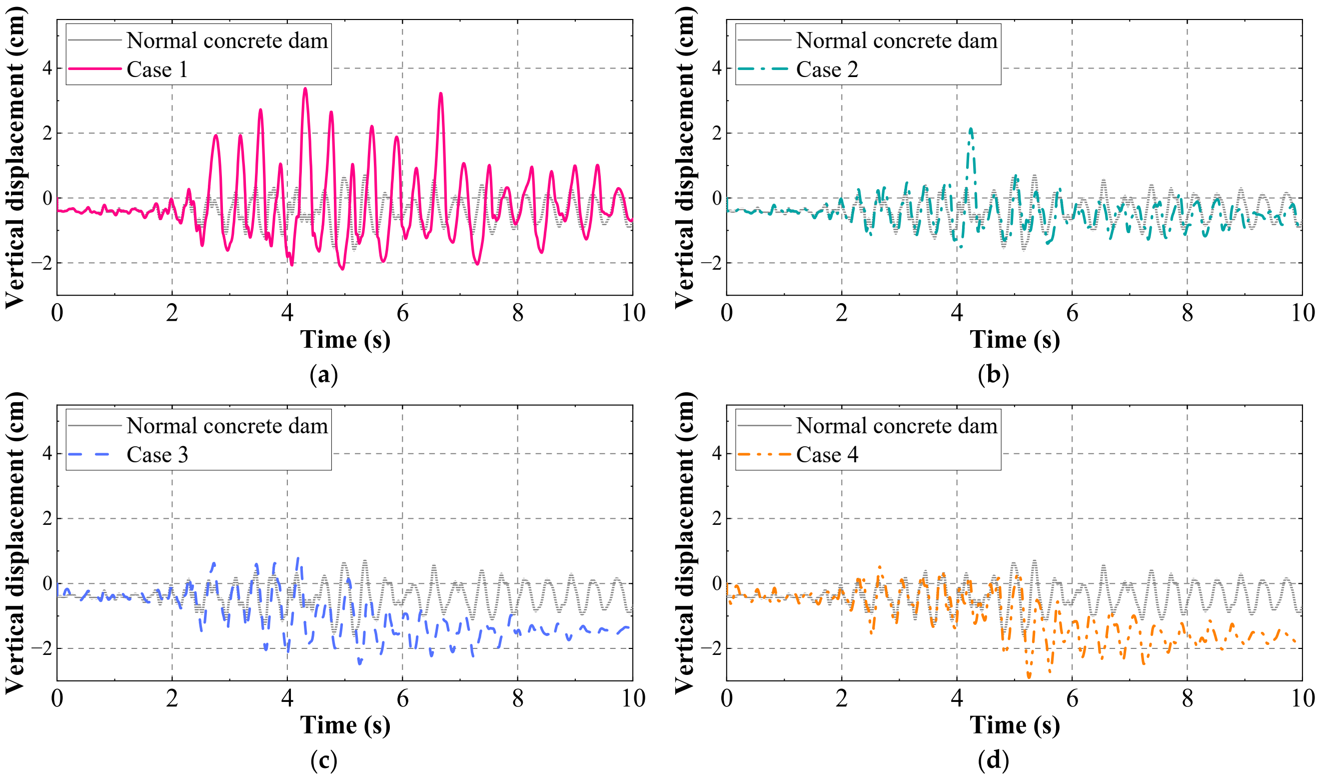

Figure 11. Vertical displacement responses of the dam crest. (**a**) Case 1; (**b**) Case 2; (**c**) Case 3; (**d**) Case 4.

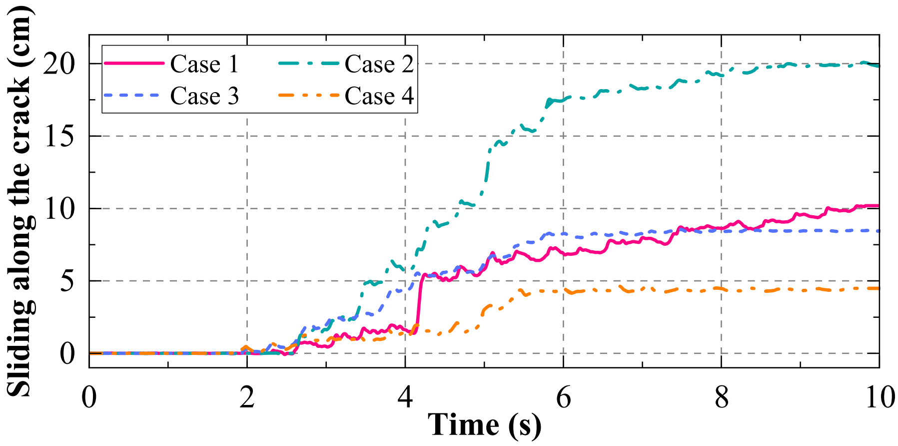

Figure 12. Sliding displacement histories of four cases.

Figures 13 and 14 show the responses of the maximum and minimum principal stresses of the dam heel for four different cases. It is clear that the peak tensile stress decreases a weak layer is present. The numerical results also reveal that the peak tensile stress of the dam heel decreases as the position of the weak layer is lowered. The reason is that the stress of the dam heel is released after the failure of the weak layer occurs. Similarly, there is an obvious decline in the response of compressive stress when a weak layer is present. The rules correspond to those obtained by Gu et al. [3]. They found that the maximum and minimum stresses are only slightly decreased on the downstream surface of the dam when cold interfaces were present. From this perspective, the stress state is beneficial to the dam to some extent. According to the displacement and stress responses of the dam, it can be preliminarily inferred that the impact of the RCC layer on the seismic performance of the dam has both advantages and disadvantages.

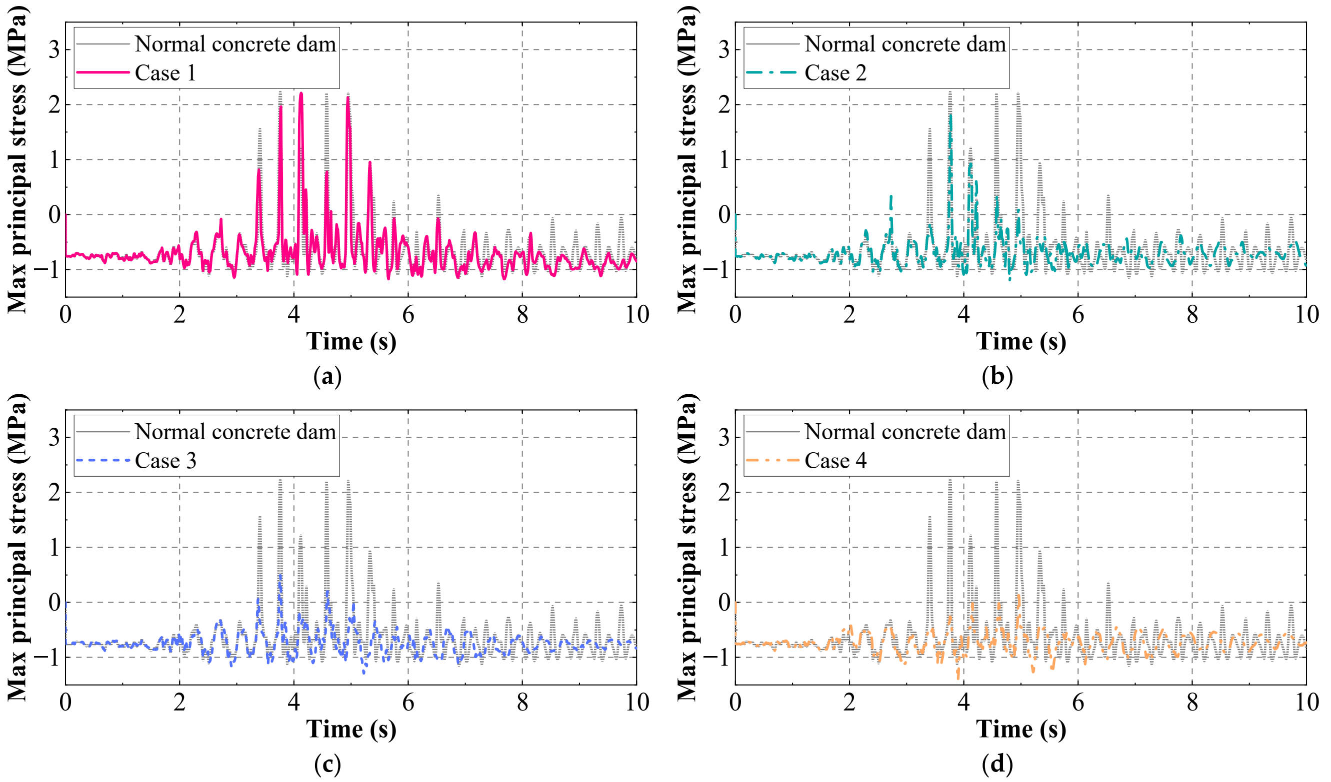

Figure 13. Maximum principal stress responses of the dam heel. (**a**) Case 1; (**b**) Case 2; (**c**) Case 3; (**d**) Case 4.

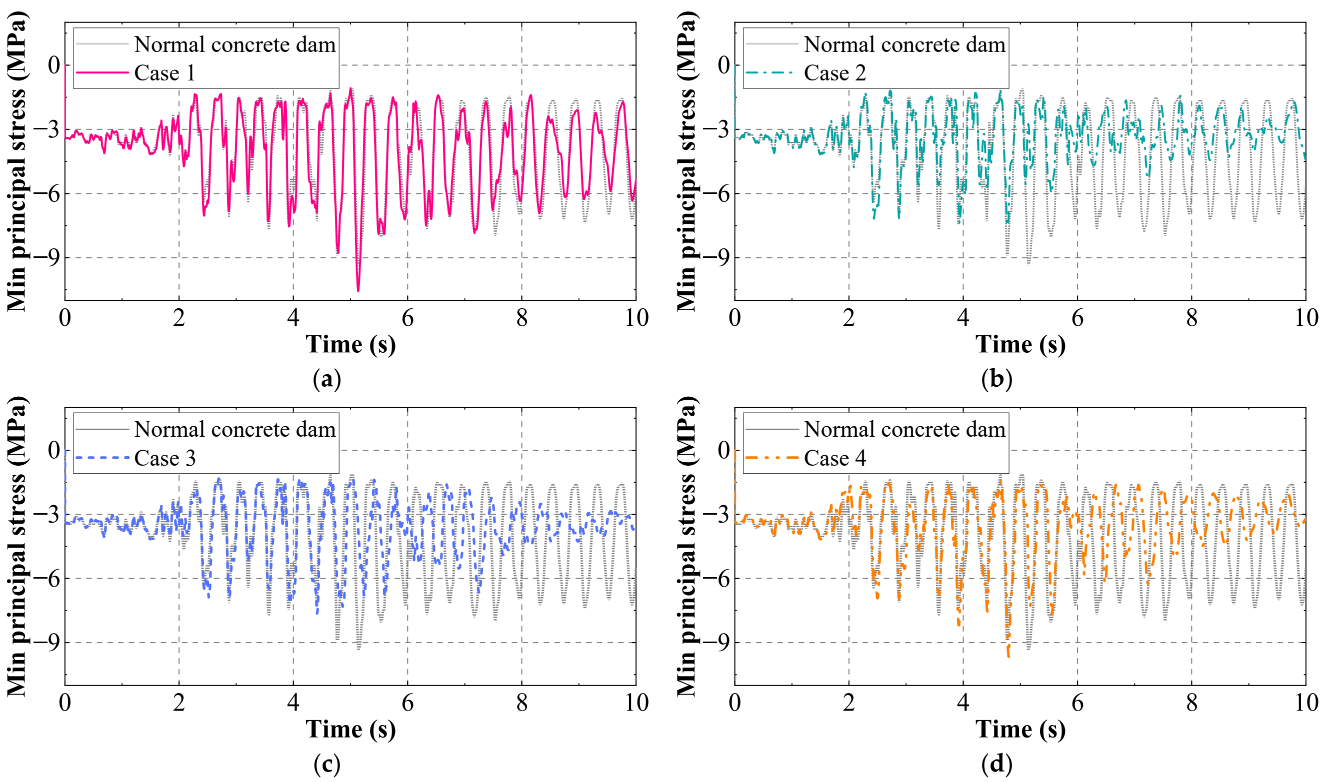

Figure 14. Minimum principal stress responses of the dam heel. (**a**) Case 1; (**b**) Case 2; (**c**) Case 3; (**d**) Case 4.

Figure 15 presents the damage-induced, plastic, and viscous energy dissipation curves for the four cases compared to the results of the normal concrete dam. As shown in Figure 15, the dam's energy dissipation is mainly manifested as a damping dissipation process, and the dissipation is increased when there is a weak layer in the dam. When a weak layer is present, the damage-induced energy dissipation shows an obvious increase. The plastic energy dissipation in Case 1 and Case 2 is slightly reduced, while the two kinds of energy dissipation are prominently increased in Case 3 and Case 4 since the upper dam block swings more violently and the plastic damage of the dam is more serious. In general, the weak layer in the dam has an obvious influence on the energy dissipation.

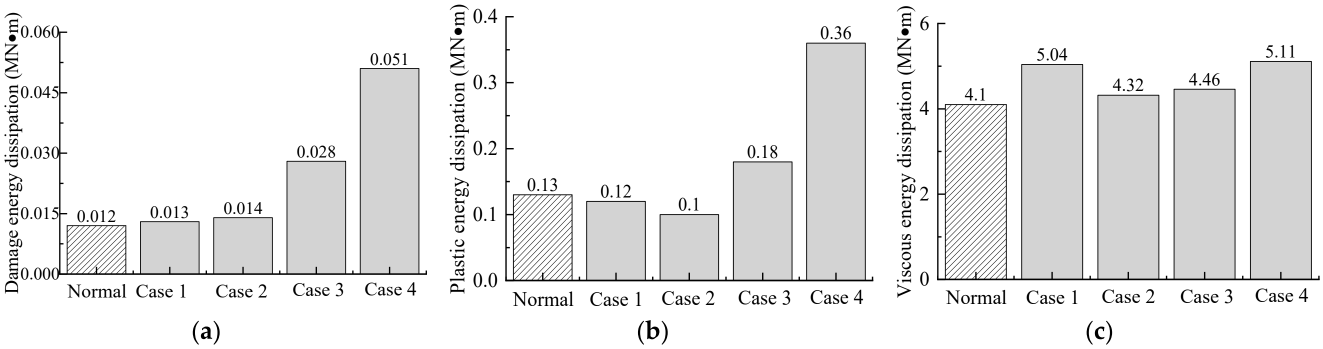

Figure 15. Comparison of the energy dissipation in different cases. (**a**) Damage energy dissipation; (**b**) plastic energy dissipation; (**c**) viscous energy dissipation.

5.2. Failure Characteristics of the Dam

The damage profiles of the Guandi dam for the different cases are given in Figures 16 and 17. Figure 16 displays the tensile damage propagation without RCC layers. When the weak layer is not present, the tensile damage to the dam mainly appears in two zones; namely, the downstream slope change and the interface between the two materials C15 and C20. The initial damage begins to propagate around the elevation, at which point the slope of the downstream face changes abruptly, mainly caused by the concentration of tensile stress. Then the initial damage extends obliquely to the inside of the dam body under the influence of the tensile stress caused by the bending of the dam body, the downward stress caused by the weight of the dam itself, and the shear stress caused by the inertia force. After nearly two thirds of the dam section width has been occupied by the crack, it spreads horizontally upstream. The interface between the two materials is also damaged along the layer.

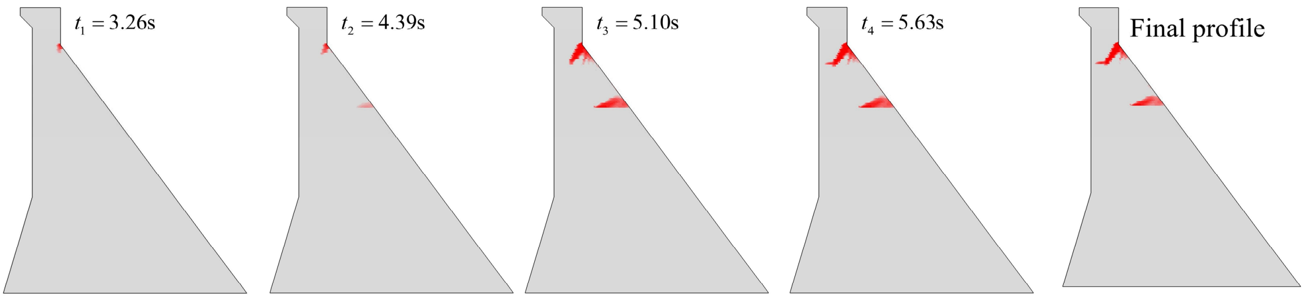

Figure 16. Damage evolution of the normal concrete dam during the Koyna earthquake.

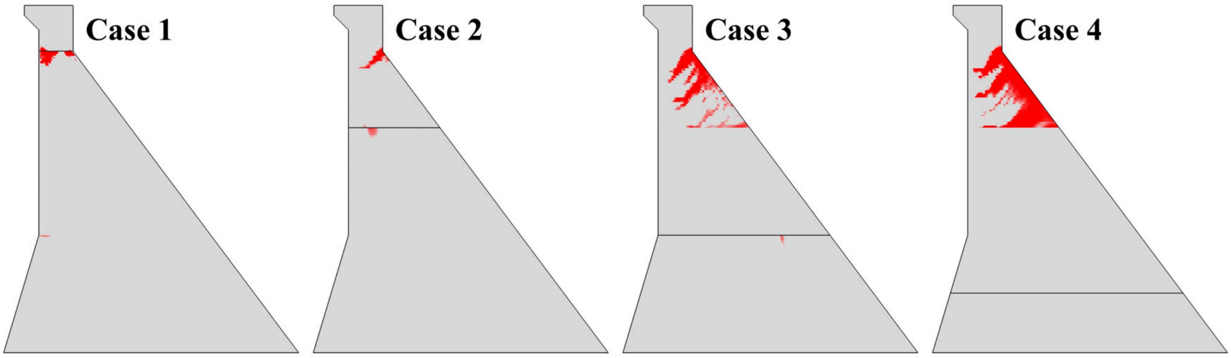

Figure 17. Damage characteristics of the dam with a weak layer for the four cases.

Figure 17 illustrates the final damage profile of the dam for the four cases. As depicted in Figure 17, the damage behaviors of the dam are significantly influenced by the weak layer. However, there are apparent differences in the damage characteristics when the weak layer is located at different elevations.

In Case 1, the tensile damage is concentrated in the weak layer. This is due to the fact that the change in the downstream slope is one of the weakest links in the dam and that the layer's strength is considerably lower than that of the noumenon. From the perspective of damage scope, the tensile damage area of this case is smaller than that of the normal concrete dam. However, since the dam head is the weak part of the dam, the concentrated damage in this area will easily lead to the generation of penetrating cracks, which is not conducive to the stability of the dam head. It should be highlighted that severe failure at the dam head should be avoided when there are frequent earthquakes, but it is acceptable when earthquakes are rare, since the requisite reparative measures are confined to a small portion of the dam. In Case 2, the damage occurs near the downstream slope change, while there is little damage to the layer. The overall damage degree is lower than that of the normal concrete dam due to the strong slipping behavior of the weak layer. Additionally, the weak layer has a minor damaged area. In Case 3 and Case 4, apart from the damage near the downstream slope change and the interface of two materials, there are also cracks generated in the downstream face. Noticeable cracks develop in the downstream surface, which spread horizontally in the direction of the upstream face after extending obliquely about halfway along the breadth of the dam section. Tensile damage also occurs at the weak layer in Case 3. Especially in Case 4, extensive damage occurs in the upper regions of the downstream face. Additionally, the energy dissipation shown in the previous subsection is in accordance with the failure mode and the damage degree of the dam. The main reason for the difference between Case 3 and Case 4 is that the location of the weak layer will affect the seismic wave propagating upward from the dam foundation. The stability of the bottom of the dam is better, and the bonding capacity of the weak layer is stronger. As a result, the stress release of the cohesive elements will lead to different degrees of damage on the upper part of the dam.

Based on the analyses above from the aspects of the seismic responses and the failure characteristics, it can be inferred that the existence of a weak layer has a significant impact on the anti-seismic capacity of the dam. The defects of the weak RCC layer will change the dam's response results and failure mode, and significantly increase the degree of deformation and the sliding of the dam. What is more, the location of the weak layer also influences the response results of the dam during a strong earthquake. As a result, it may be concluded that weak layer effects must be taken into account in the seismic design of RCC dams and attention shall be paid to the combination quality of the weak layer during construction. Furthermore, while assessing the influence of weak layers, it is vital to examine whether the responses are acceptable during earthquakes of different intensities, as the performance needs of dams vary depending on the conditions.

5.3. Damage Characteristics of the Dam with Higher Strength Grade Concrete in the Upper Part

The dynamic analysis results above show that tensile failure occurs near the change in the downstream slope, which is attributed to the relatively low stiffness of the upper part. Therefore, the strength grade of the upper concrete is replaced with C20. The dam's damage profiles in four cases are illustrated in Figure 18. It is clear that the damage to the dam has been significantly reduced compared to the results in Figure 17. From the perspective of the scope of dam tensile damage, a higher strength of concrete can lead to less damage to the dam. However, the reduction in dam ductility and the increase in construction cost caused by increasing concrete strength should also be considered comprehensively. It is suggested that concrete with both high strength and high ductility should be taken into account, as this can effectively prevent cracking.

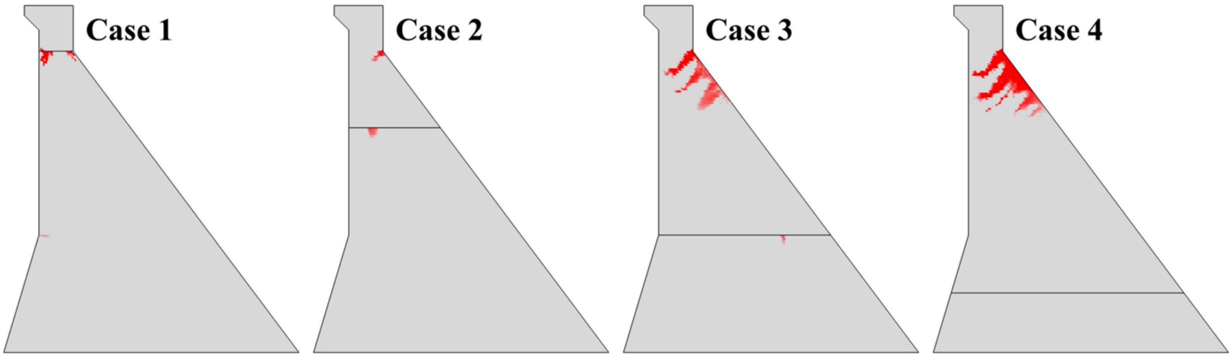

Figure 18. Damage characteristics of the dam with higher strength grade concrete in the upper part.

5.4. Damage Characteristics of the Dam with a Well-Bonded Layer

This subsection preliminarily discusses the influence of layer parameters on the damage modes of the dam. The sole difference between the parameters used in this subsection and those in Section 4.2 is that the layer parameters are the same as the concrete noumenon, which are not considered weak. It can be seen from Figure 19 that increasing the layer strength has a limited effect on the damage characteristics of the dam. As mentioned in the previous subsection, the benefits and drawbacks of simply increasing layer strength need to be evaluated in the future through more in-depth investigation.

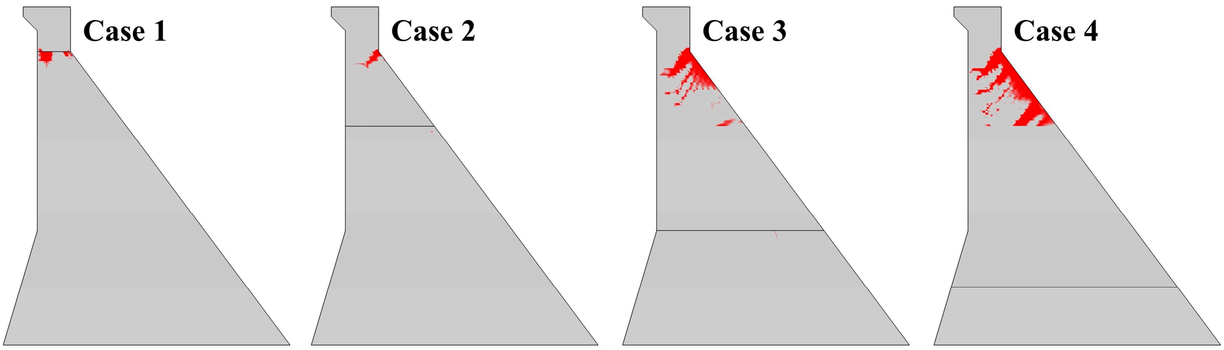

Figure 19. Damage characteristics of the dam with a well-bonded layer.

6. Influence of Well-Bonded RCC Layers Set at Intervals on Seismic Performance of the Dam

As introduced before, RCC dams are usually built lift by lift, and the RCC layers are processed properly to control the combination quality between adjacent concreting lifts. There are many methods for interlayer treatments to increase the bond strength of the RCC layers, such as paving mortar and cement mortar after jetting hair and exposing aggregate without film. In the previous section, only one weak layer was considered in each case and the strength parameters of the layer were taken as 75% of the RCC noumenon. An initial inference is drawn in Section 5.4 that a dam with a well-bonded layer acts differently from the normal concrete dam due to the anisotropy. This section aims to simulate the actual situation of RCC dams and evaluate the effects of well-bonded RCC layers on the seismic behavior of the Guandi dam. The simulation of the interfaces in the dam was simplified based on the characteristics of roller-compacted concrete placement, i.e., intermittent rising layer by layer. Therefore, the RCC layers were set at 3 m intervals along the height of the dam. Not only can this simplification reflect effectively the stratification characteristics of RCC, but it can also control the computational cost to a reasonable extent. It should be noted that inclined layers were not considered, as shown in Figure 20. Supposing that all RCC layers were well processed during the construction, the tensile strength, stiffness, and fracture energy were all the same as those of RCC noumenon to simulate the good combination quality of the interlayers. The zoning of the dam was the same as described in Section 4.1. The properties of the dam concrete can also be found in Table 1. The boundary conditions, properties of the foundation, reservoir water and concrete noumenon, and seismic loading were all kept constant.

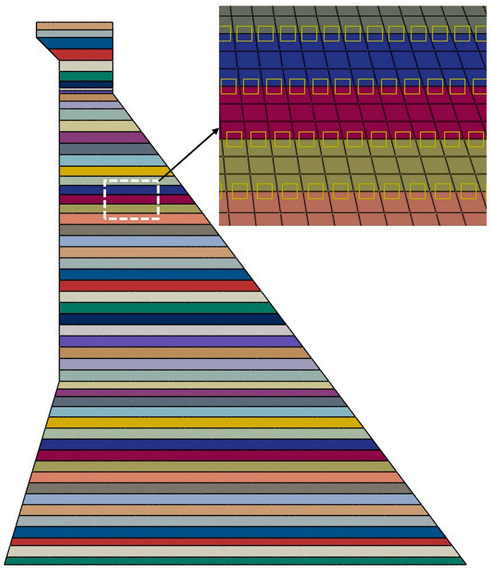

Figure 20. Schematic diagram of the dam with RCC layers every 3m along the dam by zero-thickness cohesive elements.

6.1. Static and Modal Analysis

The static analysis of the Guandi dam is here studied before the dynamic analysis. Only the weight of the dam itself and hydrostatic pressure are considered in this analysis. The displacement and stress distribution of the dam with and without the effects of RCC layers are compared in Figure 21. The units of principal stress and displacement are Pa and m, respectively. The analysis shows that RCC layers have a limited influence on the distribution of the stress of the dam, while the values of the principal stress of the dam are mainly affected. For compressive stress, the distribution of the two situations is generally similar. The maximum compressive stress values are both located at the dam toe and the values are 13.6 MPa and 10.7 MPa, respectively, which reduce by 21% when RCC layers are present. A slight increase in the maximum horizontal and vertical displacement is observed when the RCC layers are taken into account.

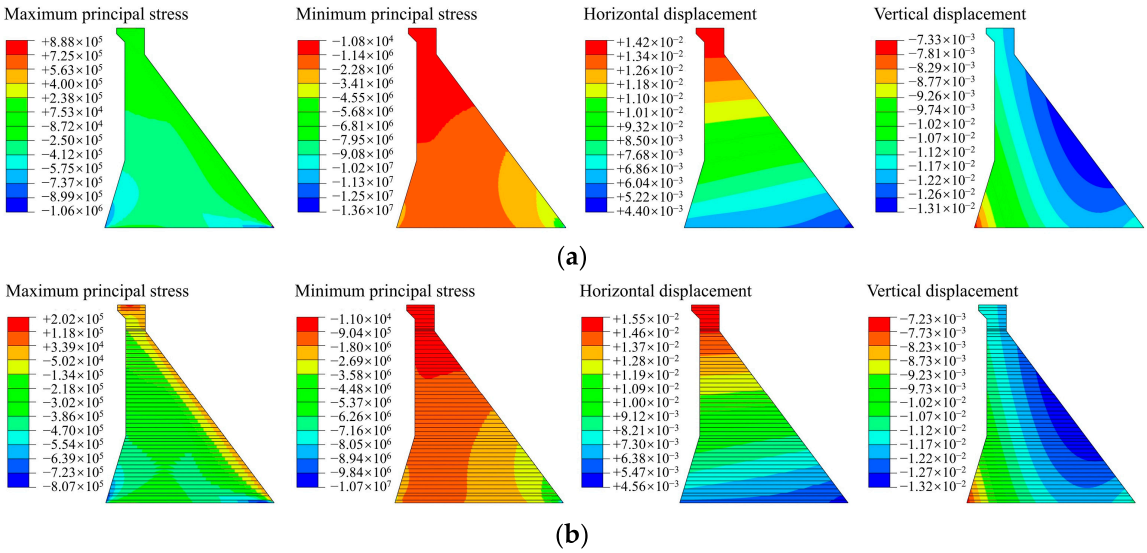

Figure 21. Principal stress and displacement responses of the dam in static analysis. (**a**) Without RCC layers; (**b**) with RCC layers.

Figure 22 shows the first five order modes and modal frequencies of the dam. It can be concluded that there is no significant difference in vibration modes and natural frequencies, denoting that the RCC layers have little impact on the dam's natural vibration characteristics, which is in accordance with the results presented in [3].

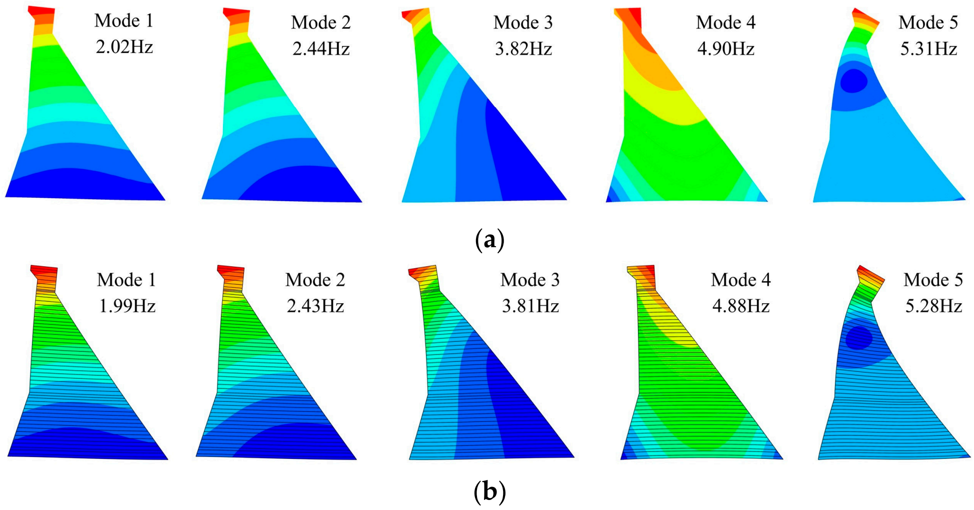

Figure 22. The first five order modes and natural frequencies. (**a**) Without RCC layers; (**b**) with RCC layers.

6.2. Seismic Response Analysis

When the strength parameters of the RCC layers were equal to those of the RCC body, the displacement time histories of the dam crest were plotted, as in Figure 23. As depicted in the figures, the peak displacement in the horizontal and vertical directions increases when RCC layers are present. At the same time, unrecovered residual deformation in the stream direction forms when RCC layers are present. Additionally, there is a gradual lag in the response curves. The results indicate that the dam's displacement response will be enhanced when RCC layers are taken into account. In practice, it is essential but difficult to ensure the RCC aggregates of adjacent layers to overcome their mutual friction and ensure a completely monolithic structure [50]. Consequently, the RCC dam is an anisotropic body even if the weak layers are well processed during construction, which leads to the huge differences in displacement response of the dam crest.

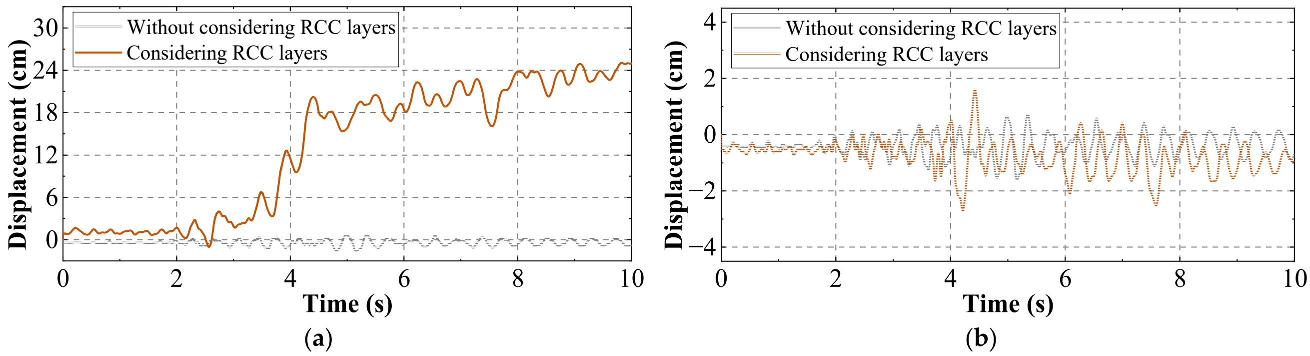

Figure 23. Displacement time histories of the dam crest. (**a**) Horizontal direction; (**b**) vertical direction.

The maximum and minimum principal stresses near the downstream slope change, with and without RCC layers, are depicted in Figure 24. The maximum tensile stresses of the two cases both exceed the tensile strength of the concrete. The maximum values of tensile and compressive stresses are reduced to a certain extent when RCC layers are present. When not considering RCC layers, the tensile stress of the selected element is not released after the failure occurs. On the contrary, the stress is almost released when RCC layers are present, and the residual stress is relatively small at the end of the earthquake duration. If the residual stress in the dam concrete is too large, the superposition of the residual tensile stress may cause the generation or expansion of cracks when the overall stress is affected by temperature drop and other factors. In addition, it may also cause the creep deformation of concrete. From this point of view, the stress state of the slope change with RCC layers considered is more favorable.

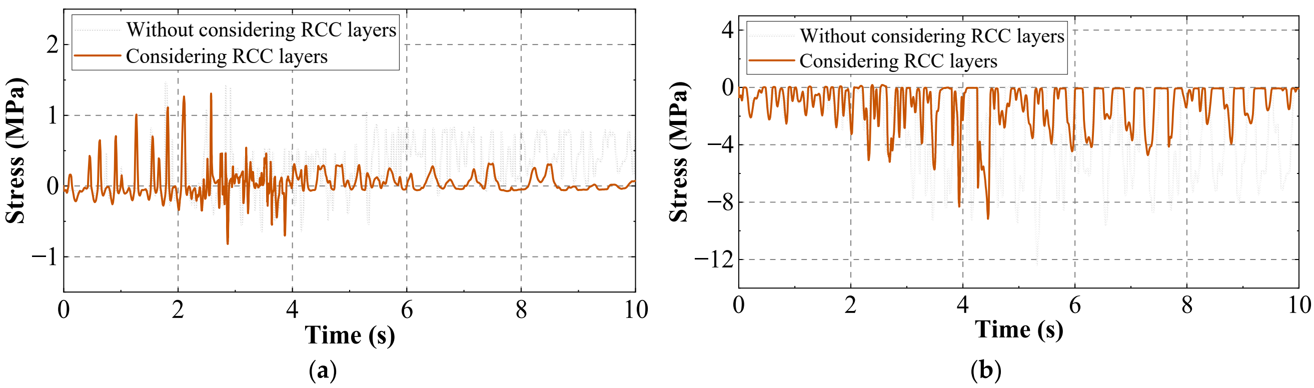

Figure 24. Stress time histories near the change in downstream slope. (**a**) Maximum principal stress; (**b**) minimum principal stress.

The energy dissipation of the two situations is also compared herein. Similarly, the energy dissipation of the dam during the strong earthquake is dominated by the damping dissipation mechanism. Figure 25 illustrates how the energy dissipation of the RCC dam differs dramatically from the normal concrete dam. The viscous energy dissipation with RCC layers is about twice that of the dam without RCC layers, whose increase range is smaller than that of the plastic and damage-induced energy dissipation. The damaged-induced energy dissipation values of the dam are 0.67 MN·m and 0.01 MN·m without and with RCC layers, respectively. Additionally, the values of plastic energy dissipation are 0.36 MN·m and 0.13 MN·m, respectively. For these two kinds of energy dissipation, the amplitude of increase reaches tens of times, which indicates that the existence of the RCC layers will cause the plastic deformation of the dam to increase significantly and lead to more severe damage, even though the weak layers have been treated well.

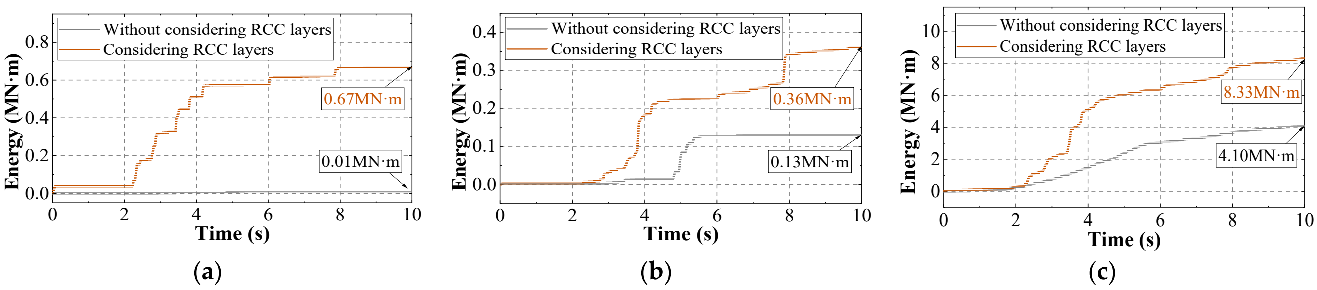

Figure 25. Comparison of the energy dissipation. (**a**) Damage energy dissipation; (**b**) plastic energy dissipation; (**c**) viscous energy dissipation.

6.3. Damage Propagation Analysis

Figures 26 and 27 depict the damage evolution process of the dam when RCC layers are present and the ultimate damage profiles of the dam. The results illustrate that the RCC layers have an obvious effect on the failure characteristics of the dam. When the RCC layers are taken into consideration, tensile damage first occurs at the downstream slope change due to the stress concentration. Then the interlayer between the two materials C15 and C20 begins to sustain damage. Because of the interaction of the adjacent RCC layers, the damage gradually expands to the adjacent layer. Finally, a small area of the upper part of the downstream face is damaged.

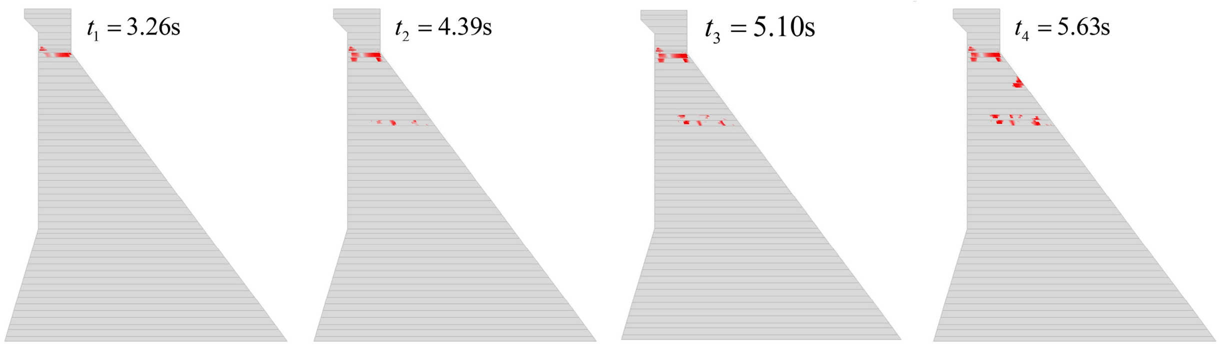

Figure 26. Damage evolution process of the dam with RCC layers.

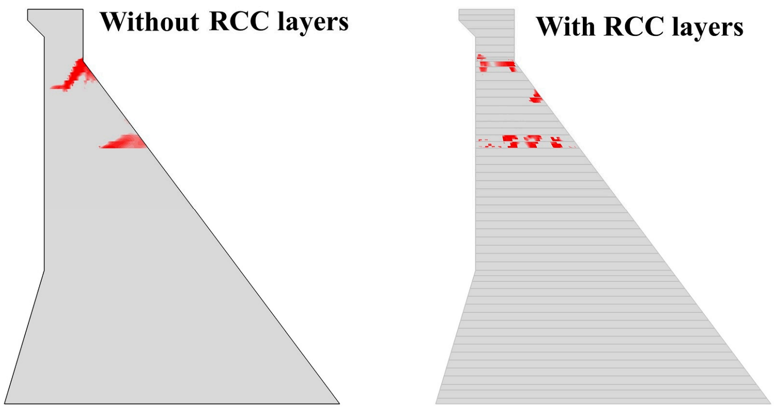

Figure 27. Final damage profiles with and without RCC layers.

As introduced in Section 5.2, there are two main damage zones in the normal concrete dam: one at the interface of the two materials and one in the upper part of the dam. The damage in the upper part of the dam starts from the downstream slope change, then extends obliquely due to the stress, and finally develops horizontally to the upstream. Different from the normal concrete dam, there are three main damaged areas in the dam. In addition to the downstream slope change and materials interface, the position near the downstream face is also damaged. Another significant difference is that the progression of damage is horizontal in the RCC dam and diagonal in the normal concrete dam.

According to the results obtained in this section, well-bonded RCC layers have obvious effects on the seismic responses of the dam. The numerous layers make the dam behave as an anisotropic body. When RCC layers are present, the overall stiffness and the natural frequencies of the dam decrease, indicating more ductility. The displacement responses of the dam increase significantly, while the stress responses are reduced. The RCC interlayers are the typical weak link of the Guandi RCC dam that will be damaged during the action of seismic loads. Under the same ground motion, the damage is more likely to occur at the RCC layers. Therefore, much attention should be paid to the effects of RCC layers on the dynamic performance of the dam.

7. Conclusions

In this paper, the influence of weak layers in an RCC gravity dam on the seismic performance of the dam was studied. The 2D finite element model of the Guandi RCC gravity dam was established with the zero-thickness cohesive element method simulating the RCC layers. An experiment regarding the influence of the weak layer at different elevations on the seismic responses of the dam was first conducted. Subsequently, the effects of well-bonded RCC layers which were set every 3m along the dam on the static, and modal characteristics were investigated. On this basis, their effects on the seismic responses of the dam were further studied. The following conclusions are drawn.

(1) The weak layer will influence the anti-seismic capacity of the RCC gravity dam. The nonlinear dynamic responses vary when the weak layer is at different elevations of the dam. Higher peak and irrecoverable displacement of the dam crest can be observed when a weak layer is present, while the maximum tensile stress of the dam heel is reduced due to the stress release. In summary, the structural behavior of the dam is affected by the weak layer, which has both advantages and disadvantages.

(2) The damage modes of the Guandi dam under seismic input without RCC layers include a diagonal crack near the downstream slope change and a horizontal crack in the interface between the two materials in the upper part. The existence of the weak layer leads to different damage characteristics of the dam, and the damage mode is related to the position of the weak layer. Increasing the strength of concrete in the upper dam body or the layer can reduce the damage degree of the dam to a certain extent, while the ductility of the dam is reduced.

(3) The RCC layers are usually processed in the construction to ensure combination quality. Well-bonded RCC layers cause the anisotropy and higher ductility of the RCC dam. An enhanced displacement response and a smaller stress response can be observed. Additionally, the energy dissipation increases significantly when RCC layers are present. The damage to the dam is significantly changed and is more likely to occur at RCC layers under the same seismic input.

Based on the available conclusions, it should be emphasized that the influence of RCC layers on the seismic responses of the dam is complicated and cannot be lumped together. As indicated in [3], it is important to ensure the bonding quality of the layers during construction to avoid considerable sliding along the construction interfaces during potential earthquakes. Meanwhile, during strong earthquakes, the localization effect of the layer on tensile damage may have a favorable impact on post-earthquake repair. The impact of measures to merely improve material strength on the anti-seismic capacity of dams must be thoroughly assessed after considering the benefits and drawbacks.

The aforementioned conclusions may not apply to all RCC gravity dams and ground motions since they were drawn from the Guandi RCC gravity dam's response results corresponding to a specific earthquake. Future research will include incremental dynamic analysis and a more comprehensive ground motion database to obtain the possible failure modes of the dam when considering the RCC layers. Additionally, an appropriate evaluation system will be carried out to quantitatively analyze the effect of RCC layers.

In addition, the influence of the cohesive model parameters on the characteristics of RCC layers and the seismic performance of the dams will be further studied to find the key factors affecting the seismic responses of the dam.

Author Contributions: Conceptualization, G.W. and W.L.; methodology, G.W. and W.L.; software, A.L.; formal analysis, A.L.; investigation, A.L.; resources, M.C.; writing—original draft preparation, A.L.; writing—review and editing, G.W.; visualization, P.Y.; supervision, W.L. All authors have read and agreed to the published version of the manuscript.

Funding: This research was funded by the National Key Research and Development Program of China, grant number 2022YFC3005402; by the National Natural Science Foundation of China, grant number 52179140 and 51939008; and by the Natural Science Funds of Hubei Province for Distinguished Young Scholar, grant number 2021CFA093.

Data Availability Statement: Not applicable.

Acknowledgments: The authors gratefully appreciate the supports from the National Key Research and Development Program of China (No. 2022YFC3005402), the National Natural Science Foundation of China (Nos. 52179140 and 51939008), and the Natural Science Funds of Hubei Province for Distinguished Young Scholar (No. 2021CFA093).

Conflicts of Interest: The authors declare no conflict of interest.

References

1. Zhao, E.; Li, B. Evaluation method for cohesive crack propagation in fragile locations of RCC dam using XFEM. *Water* **2021**, *13*, 58. [CrossRef]
2. Chen, S.H. *Hydraulic Structures*; Springer: Berlin/Heidelberg, Germany, 2016. [CrossRef]
3. Gu, C.; Wang, S.; Bao, T. Influence of construction interfaces on dynamic characteristics of roller compacted concrete dams. *J. Cent. South Univ.* **2015**, *22*, 1521–1535. [CrossRef]
4. Ayari, M.L.; Saouma, V.E. A fracture mechanics based seismic analysis of concrete gravity dams using discrete cracks. *Eng. Fract. Mech.* **1990**, *35*, 587–598. [CrossRef]
5. Bhattacharjee, S.S.; Léger, P. Seismic cracking and energy dissipation in concrete gravity dams. *Earthq. Eng. Struct. Dyn.* **1993**, *22*, 991–1007. [CrossRef]
6. Lee, J.; Fenves, G.L. A plastic-damage concrete model for earthquake analysis of dams. *Earthq. Eng. Struct. Dyn.* **1998**, *27*, 937–956. [CrossRef]
7. Daneshyar, A.; Ghaemian, M. Seismic analysis of arch dams using anisotropic damage-plastic model for concrete with coupled adhesive-frictional joints response. *Soil Dyn. Earthq. Eng.* **2019**, *125*, 105735. [CrossRef]
8. Tidke, A.R.; Adhikary, S. Seismic fragility analysis of the Koyna gravity dam with layered rock foundation considering tensile crack failure. *Eng. Fail. Anal.* **2021**, *125*, 105361. [CrossRef]
9. Wang, G.; Wang, Y.; Lu, W.; Zhou, C.; Chen, M.; Yan, P. XFEM based seismic potential failure mode analysis of concrete gravity dam-water-foundation systems through incremental dynamic analysis. *Eng. Struct.* **2015**, *98*, 81–94. [CrossRef]
10. Wang, G.; Lu, W.; Zhou, C.; Zhou, W. The influence of initial cracks on the crack propagation process of concrete gravity dam-reservoir-foundation systems. *J. Earthq. Eng.* **2015**, *19*, 991–1011. [CrossRef]
11. Haghani, M.; Neya, B.N.; Ahmadi, M.T.; Amiri, J.V. Combining XFEM and time integration by α-method for seismic analysis of dam-foundation-reservoir. *Theor. Appl. Fract. Mech.* **2020**, *109*, 102752. [CrossRef]
12. Haghani, M.; Neya, B.N.; Ahmadi, M.T.; Amiri, J.V. A new numerical approach in the seismic failure analysis of concrete gravity dams using extended finite element method. *Eng. Fail. Anal.* **2022**, *132*, 105835. [CrossRef]
13. Haghani, M.; Neya, B.N.; Ahmadi, M.T.; Amiri, J.V. Comparative study of smeared crack and extended finite element method for predicting the crack propagation in concrete gravity dams. *J. Earthq. Eng.* **2021**, *26*, 8577–8610. [CrossRef]
14. Mirzayee, M.; Khaji, N.; Ahmadi, M.T. A hybrid distinct element–boundary element approach for seismic analysis of cracked concrete gravity dam–reservoir systems. *Soil Dyn. Earthq. Eng.* **2011**, *31*, 1347–1356. [CrossRef]
15. Sharma, V.; Fujisawa, K.; Murakami, A. S Space–time FEM with block-iterative algorithm for nonlinear dynamic fracture analysis of concrete gravity dam. *Soil Dyn. Earthq. Eng.* **2020**, *131*, 105995. [CrossRef]
16. Wang, Y.; Wu, Z.; Qu, F.; Zhang, W. Numerical investigation on crack propagation process of concrete gravity dams under static and dynamic loads with in-crack reservoir pressure. *Theor. Appl. Fract. Mech.* **2022**, *117*, 103221. [CrossRef]
17. Yilmazturk, S.M.; Arici, Y.; Binici, B. Seismic assessment of a monolithic RCC gravity dam including three dimensional dam-foundation-reservoir interaction. *Eng. Struct.* **2015**, *100*, 137–148. [CrossRef]
18. Chen, D.; Yang, Z.; Wang, M.; Xie, J. Seismic performance and failure modes of the Jin'anqiao concrete gravity dam based on incremental dynamic analysis. *Eng. Fail. Anal.* **2019**, *100*, 227–244. [CrossRef]

19. Ghaedi, K.; Hejazi, F.; Ibrahim, Z.; Khanzaei, P. Flexible foundation effect on seismic analysis of roller compacted concrete (RCC) dams using finite element method. *KSCE J. Civ. Eng.* **2018**, *22*, 1275–1287. [CrossRef]
20. Wang, C.; Hao, H.; Zhang, S.; Wang, G. Influence of ground motion duration on responses of concrete gravity dams. *J. Earthq. Eng.* **2020**, *24*, 1156–1180. [CrossRef]
21. Ferguson, K.A. Risk-informed design of RCC dams under extreme seismic loading. *Water* **2023**, *15*, 116. [CrossRef]
22. Sha, S.; Lei, Z.; Zhang, X. Study on failure mechanism of roller compacted concrete gravity dams by an isotropic damage model. In Proceedings of the 2016 International Conference on Smart City and Systems Engineering (ICSCSE), Hunan, China, 25–26 November 2016; pp. 68–71. [CrossRef]
23. Rahulkumar, P.; Jagota, A.; Bennison, S.J.; Saigal, S. Cohesive element modeling of viscoelastic fracture: Application to peel testing of polymers. *Int. J. Solids Struct.* **2000**, *37*, 1873–1897. [CrossRef]
24. Cornec, A.; Scheider, I.; Schwalbe, K.H. On the practical application of the cohesive model. *Eng. Fract. Mech.* **2003**, *70*, 1963–1987. [CrossRef]
25. Hillerborg, A.; Modéer, M.; Petersson, P.E. Analysis of crack formation and crack growth in concrete by means of fracture mechanics and finite elements. *Cem. Concr. Res.* **1976**, *6*, 773–781. [CrossRef]
26. Nguyen, V.P.; Nguyen, C.T.; Bordas, S.; Heidarpour, A. Modelling interfacial cracking with non-matching cohesive interface elements. *Comput. Mech.* **2016**, *58*, 731–746. [CrossRef]
27. Shu, X.; Luo, Y.; Zhao, C.; Dai, Z.; Zhong, X.; Zhang, T. Experimental study on the shear failure model for concrete under compression-shear loading. *Comput. Concr.* **2022**, *29*, 81–92. [CrossRef]
28. Paggi, M.; Ferro, G.; Braga, F. Seismic analysis of concrete gravity dams: Nonlinear fracture mechanics models and size-scale effects. *Appl. Mech. Mater.* **2011**, *82*, 374–379. [CrossRef]
29. Zhong, H.; Li, H.; Ooi, E.T.; Song, C. Hydraulic fracture at the dam-foundation interface using the scaled boundary finite element method coupled with the cohesive crack model. *Eng. Anal. Bound. Elem.* **2018**, *88*, 41–53. [CrossRef]
30. Zhu, H.; Wang, G.; Ma, Z.; Su, Y. Seismic time-history analysis of gravity dam based on nonlinear finite element method. *Appl. Mech. Mater.* **2013**, *351–352*, 1047–1051. [CrossRef]
31. Altunisik, A.C.; Sesli, H. Dynamic response of concrete gravity dams using different water modelling approaches: Westergaard, Lagrange and Euler. *Comput. Concr.* **2015**, *16*, 429–448. [CrossRef]
32. Ye, J.; Zhou, H.; Zhou, X. Hydrodynamic pressure on lateral side of dam excited by harmonic seismic vibration: A novel formulation. *Soil Dyn. Earthq. Eng.* **2023**, *164*, 107626. [CrossRef]
33. Nariman, N.A.; Lahmer, T.; Karampour, P. Uncertainty quantification of stability and damage detection parameters of coupled hydrodynamic-ground motion in concrete gravity dams. *Front. Struct. Civ. Eng.* **2019**, *13*, 303–323. [CrossRef]
34. Ya, S.; Eisenträger, S.; Qu, Y.; Zhang, J.; Kuen, T.; Song, C. Seismic analysis of post-tensioned concrete gravity dams using scaled boundary finite elements implemented as ABAQUS UEL. *Soil Dyn. Earthq. Eng.* **2023**, *164*, 107620. [CrossRef]
35. Camanho, P.P.; Davila, C.G. Mixed-mode decohesion finite elements for the simulation of delamination in composite materials. *NASA Tech. Pap.* **2002**, *211737*, 42.
36. ABAQUS. *ABAQUS User's Manual*; Dassault Systèmes Simulia Corp.: Providence, RI, USA, 2021.
37. Liu, X.; Deng, W.; Liu, B.; Liu, Q.; Zhu, Y.; Fan, Y. Influence analysis on the shear behaviour and failure mode of grout-filled jointed rock using 3D DEM coupled with the cohesive zone model. *Comput. Geotech.* **2023**, *155*, 105165. [CrossRef]
38. Du, J.; Yon, J.; Hawkins, N.; Arakawa, K.; Kobayashi, A. Fracture process zone for concrete for dynamic loading. *ACI Mater. J.* **1992**, *89*, 252–258. [CrossRef]
39. Pan, J.; Zhang, C.; Xu, Y.; Jin, F. A comparative study of the different procedures for seismic cracking analysis of concrete dams. *Soil Dyn. Earthq. Eng.* **2011**, *31*, 1594–1606. [CrossRef]
40. Qu, Y.Q.; Zou, D.; Kong, X.; Yu, X.; Chen, K. Seismic cracking evolution for anti-seepage face slabs in concrete faced rockfill dams based on cohesive zone model in explicit SBFEM-FEM frame. *Soil Dyn. Earthq. Eng.* **2020**, *133*, 106106. [CrossRef]
41. Wang, G.; Wang, Y.; Lu, W.; Yan, P.; Chen, M. Earthquake direction effects on seismic performance of concrete gravity dams to mainshock–aftershock sequences. *J. Earthq. Eng.* **2020**, *24*, 1134–1155. [CrossRef]
42. Lubliner, J.; Oliver, J.; Oller, S.; Oñate, E. A plastic-damage model for concrete. *Int. J. Solids Struct.* **1989**, *25*, 299–326. [CrossRef]
43. Pourbehi, M.S.; van Zijl, G.P. A. G.; Strasheim, J.A. v. B. Analysis of combined action of seismic loads and alkali-silica reaction in concrete dams considering the key chemical-physical-mechanical factors and fluid-structure interaction. *Eng. Struct.* **2019**, *195*, 263–273. [CrossRef]
44. Pan, X.; Wang, G.; Lu, W.; Yan, P.; Chen, M.; Gao, Z. The effects of initial stresses on nonlinear dynamic response of high arch dams subjected to far-field underwater explosion. *Eng. Struct.* **2022**, *256*, 114040. [CrossRef]
45. Yan, C.; Tu, J.; Li, D.; Guo, S.; Liang, H. The failure mechanism of concrete gravity dams considering different nonlinear models under strong earthquakes. *Shock Vib.* **2021**, *2021*, 1–17. [CrossRef]
46. Mridha, S.; Maity, D. Experimental investigation on nonlinear dynamic response of concrete gravity dam-reservoir system. *Eng. Struct.* **2014**, *80*, 289–297. [CrossRef]
47. Wang, G.; Wang, Y.; Lu, W.; Yan, P.; Zhou, W.; Chen, M. A general definition of integrated strong motion duration and its effect on seismic demands of concrete gravity dams. *Eng. Struct.* **2016**, *125*, 481–493. [CrossRef]
48. Ministry of Housing and Urban-Rural Development of the People's Republic of China. *Code for Seismic Design of Hydraulic Structures (GB 51247-2018)*; Planning Press: Beijing, China, 2018.

49. Khazaee, A.; Lotfi, V. Application of perfectly matched layers in the transient analysis of dam–reservoir systems. *Soil Dyn. Earthq. Eng.* **2014**, *60*, 51–68. [CrossRef]
50. Liu, D.; Li, Z.; Liu, J. Experimental study on real-time control of roller compacted concrete dam compaction quality using unit compaction energy indices. *Constr. Build. Mater.* **2015**, *96*, 567–575. [CrossRef]